

# Feasibility Study of Radio Frequency Current Density Imaging with Only One Rotation

Dinghui Wang<sup>1,2</sup>, Weijing Ma<sup>1,2</sup>, Tim P. DeMonte<sup>4</sup>, Adrian I. Nachman<sup>1,3</sup> and Michael L. Joy<sup>1,2</sup>

<sup>1</sup>Dept. of ECE, <sup>2</sup>IBBME and <sup>3</sup>Dept. of Mathematics, University of Toronto, <sup>4</sup>Field Metrica Inc., Toronto, ON, Canada  
dinghui.wang@utoronto.ca

**Abstract-** Radio frequency current density imaging (RF-CDI) is an imaging technique that measures current density distribution at the Larmor frequency utilizing magnetic resonance imaging (MRI). The previous implemented RF current reconstruction method is based on the single orientation condition that usually requires the applied current flowing mainly in the direction of the static magnetic field of the MR imager. However, this condition can be violated in biomedical applications. This paper proposes a new reconstruction method for RF-CDI, which does not rely on the single orientation assumption. Instead, the sample is rotated 180 degrees to collect MR data from two opposite orientations. Simulations and experiment are analyzed for the feasibility of the approach.

## I. INTRODUCTION

Based on magnetic resonance imaging (MRI), Current density imaging (CDI) measures the electrical current density distribution in the subject being imaged. The non-invasiveness and the high spatial resolution inherited from MRI makes CDI an ideal measurement of current density and current flow inside a body. At the present stage, current is usually injected externally by electrodes. According to the frequency of the injected current and hence the frequency of the current density imaged, there are two major branches of CDI technique, namely, low frequency CDI (LF-CDI) and radio frequency CDI (RF-CDI). The former measures current density in the frequency range of 1~100 Hz [1], while the latter images the Larmor frequency current density.

RF-CDI may be more applicable in clinical applications than low frequency current density imaging (LF-CDI), because considerable amount of radio frequency current can be applied to animals and human beings without stimulating nerves and muscles. There have been both in-vitro and in-vivo biomedical applications for RF-CDI [2],[3].

Previous implemented RF-CDI techniques evaluate the component of applied current density in the direction of static magnetic field  $\mathbf{B}_0$  of the MR imager. This measurement corresponds to the actual applied current component only under strict constraint, which states that the derivative of magnetic intensity due to the current along the direction of the static magnetic field of the imager is much smaller than the current flowing in that direction. This condition is called the single orientation assumption [4]. Generally, the single orientation assumption requires that the current flows mainly in

$\mathbf{B}_0$  or the z direction by convention unless specific symmetry exists. In phantom experiments, it might be practical with careful electrodes and return wire arrangement. However, in biological and clinical applications, this condition can be easily violated and this would complicate the interpretation of the experiment results.

Theoretically, all components of current density vector can be recovered using three orthogonal sample orientations [4]. However, for such orthogonal rotations, subjects which can be imaged are limited by the size of magnet. Human beings and big animals can not fit into the conventional MR imagers in three orthogonal orientations. In addition, some motion of organs and tissues tends to occur due to gravity. In this paper, we present a new reconstruction method based on a single 180-degree sample rotation. This approach would be more feasible in animal and human experiments because the longitudinal axis of a body can be parallel to the axis of imager in both orientations. Theoretical analysis shows that one component of the current can be fully calculated. Simulations as well as one RF-CDI experiment are presented to verify the reconstruction formula.

## II. THEORY

The theory of RF-CDI technology stems from generalized Ampere's law. In phasor form, it is

$$\nabla \times \mathbf{H} = (\sigma + j\omega\epsilon)\mathbf{E} = \mathbf{J}, \quad (1)$$

where  $\mathbf{J}$  is the total current density including both the conduction and the displacement current density. Assume that the static magnetic field  $\mathbf{B}_0$  is in the direction of z axis. For generality, the transverse component of magnetic field yielded by the current is treated as an elliptically polarized field, which is composed of a right circularly polarized field and a left circularly polarized field

$$\begin{aligned} \mathbf{H}_{xy} &= H_x \mathbf{a}_x + H_y \mathbf{a}_y \\ &= \frac{1}{2}(H_x + jH_y)(\mathbf{a}_x - j\mathbf{a}_y) + \frac{1}{2}(H_x - jH_y)(\mathbf{a}_x + j\mathbf{a}_y) \end{aligned} \quad (2)$$

The first term in (2) is the right circularly polarized field and the second term is the left circularly polarized field. Assume that  $\hat{H}_l$  represents the instantaneous vector of the left circularly polarized component and that it is oriented  $-\theta_l$  with respect to

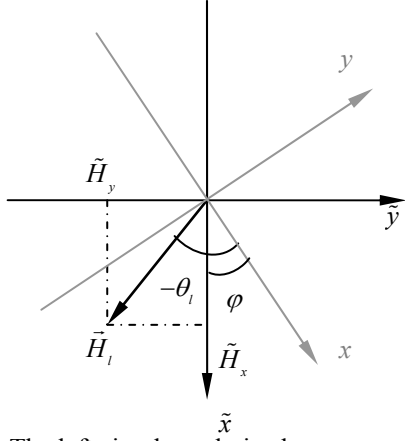


Fig. 1. The left circular polarized components in the rotating frame defined by the transmission coil

$x$  axis of the lab frame at time  $t = 0$  as shown in fig.1. In the rotating frame defined by the transmission coil denoted by  $(\tilde{\mathbf{a}}_x, \tilde{\mathbf{a}}_y)$ ,  $\tilde{H}_l$  will remain static. Suppose  $\tilde{\mathbf{a}}_x$  is at an angle  $\varphi$  with respect to  $\mathbf{a}_x$  (fig. 1). Then the lab frame phasor  $H_x$  and  $H_y$  is related to the rotating frame components  $\tilde{H}_x$  and  $\tilde{H}_y$  by

$$\frac{1}{2}(H_x - jH_y) = (\tilde{H}_x - j\tilde{H}_y)e^{-j\varphi}. \quad (3)$$

$\varphi$  can be approximately constant when a bird cage coil is used to image a relatively small sample and the static field  $\mathbf{B}_0$  is not very high. Combing (3) with  $\nabla \cdot \mathbf{H} = 0$ , we have

$$J_z e^{j\varphi} = 2 \left( \frac{\partial \tilde{H}_y}{\partial x} - \frac{\partial \tilde{H}_x}{\partial y} \right) + 2j \left( \frac{\partial \tilde{H}_x}{\partial x} + \frac{\partial \tilde{H}_y}{\partial y} \right) + j \frac{\partial H_z}{\partial z} e^{j\varphi}. \quad (4)$$

When  $|\partial H_z / \partial z| \ll |J_z|$ , the last term can be ignored. This is the single orientation assumption. With this assumption current density along  $z$  direction is estimated by

$$J_z e^{j\varphi} = 2 \left( \frac{\partial \tilde{H}_y}{\partial x} - \frac{\partial \tilde{H}_x}{\partial y} \right) + 2j \left( \frac{\partial \tilde{H}_x}{\partial x} + \frac{\partial \tilde{H}_y}{\partial y} \right), \quad (5)$$

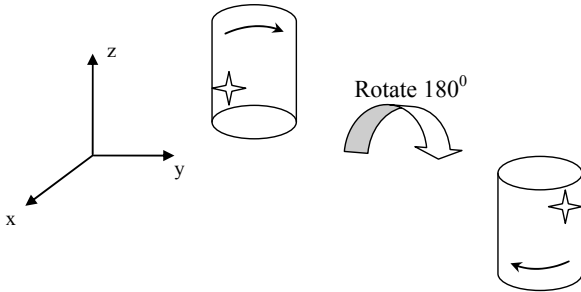


Fig. 2. Illustration of sample rotation in  $yz$  plane. The arrow on the cylinder represents a right circularly polarized component at the original position. It becomes left circularly polarized after the rotation.

where the rotating frame components  $(\tilde{H}_x, \tilde{H}_y)$  can be extracted by RF-CDI imaging methods [4],[5]. Therefore,  $J_z$  is estimated with an additional relative phase  $\varphi$ .

Now consider rotating the sample around lab frame  $x$  axis 180 degrees as illustrated in fig.2. The original right circularly polarized component in the transverse plane according to the imager coordinates becomes the left circularly polarized component after rotation. Therefore, with the same RF-CDI data acquisition, we should be able to measure the right circularly polarized field. We have

$$\frac{1}{2}(H_x + jH_y) = (\tilde{H}_x^\pi - j\tilde{H}_y^\pi)e^{-j\varphi}, \quad (6)$$

where the superscript  $\pi$  in  $\tilde{H}_x^\pi$  indicates that it is obtained after rotation. Similarly, superscript 0 is used to indicate the data collected at the original position. Assume that  $\varphi$  dose not change after rotation, then due to (3) and (6),

$$H_x = \left( (\tilde{H}_x^0 + \tilde{H}_x^\pi) - j(\tilde{H}_y^0 + \tilde{H}_y^\pi) \right) e^{-j\varphi} \quad (7)$$

and

$$H_y = \left( (\tilde{H}_y^0 - \tilde{H}_y^\pi) - j(\tilde{H}_x^0 - \tilde{H}_x^\pi) \right) e^{-j\varphi}. \quad (8)$$

Insert (7) and (8) to (1), we obtain

$$J_z e^{j\varphi} = \left( \frac{\partial \tilde{H}_y^0}{\partial x} - \frac{\partial \tilde{H}_x^0}{\partial y} - \frac{\partial \tilde{H}_y^\pi}{\partial x} - \frac{\partial \tilde{H}_x^\pi}{\partial y} \right) + j \left( \frac{\partial \tilde{H}_x^0}{\partial x} + \frac{\partial \tilde{H}_y^0}{\partial y} - \frac{\partial \tilde{H}_x^\pi}{\partial x} + \frac{\partial \tilde{H}_y^\pi}{\partial y} \right), \quad (9)$$

which means  $J_z$  can be reconstructed with an relative angle  $\varphi$  with respect to the lab frame.

### III. SIMULATION VERIFICATION

#### A. Methods

Two models were simulated as shown in fig.3 (a) and fig.4 (a). The electromagnetic fields were computed by 3-D FDTD with spatial resolution 2 by 2 by 2 mm. Sinusoidal RF current at 64MHz was applied through electrodes and wires. Steady-state responses in time domain were then converted to phasor form.

In the reconstruction process, the rotating frame components  $(\tilde{H}_x^0, \tilde{H}_y^0)$  were calculated by (3). Then the whole set of electromagnetic field vectors was rotated 180 degrees with respect to  $x$  axis of the lab frame and  $(\tilde{H}_x^\pi, \tilde{H}_y^\pi)$  calculated. Finally,  $J_z$  was computed by (5) and (9) respectively. The reconstructed  $J_z$  magnitudes were compared to the one simulated directly from the FDTD model by relative error  $\left| \left| J_z^{rec} \right| - \left| J_z^s \right| \right| / \left| J_z^s \right|$ .  $J_z^{rec}$  is reconstructed current density and  $J_z^s$  is the simulated one. The map of  $|\partial H_z / \partial z| / |J_z|$  was also computed. Sobel template was used in spatial derivative calculations.

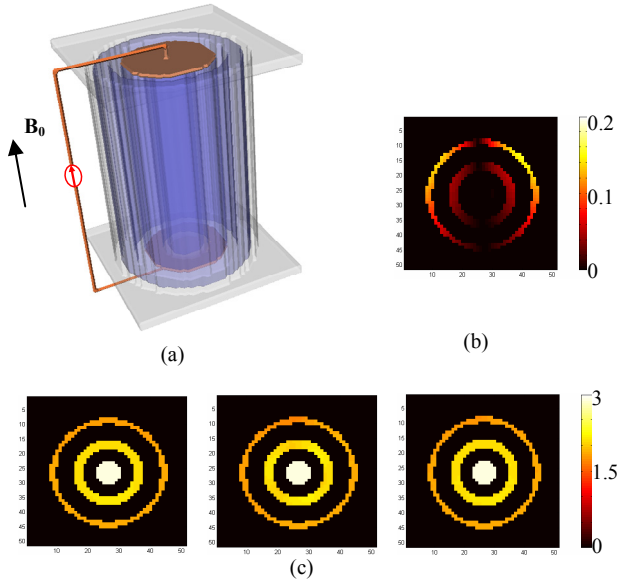


Fig. 3. Simulation model and results for model 1

- (a) Simulation model 1
- (b) Map of  $|\partial H_z / \partial z| / |J_z|$
- (c) Magnitude of  $J_z$  in logarithm scale
  - Left: computed directly from simulation
  - Middle: reconstructed by (5)
  - Right: reconstructed by (9)

### B. Results

Model 1 is a multi-chamber phantom composed of three plastic tubes. The centre part of the phantom is filled with doped saline of conductivity  $\sigma = 1.48$  S/m and relative permittivity  $\epsilon_r = 80.4$ . The other two annular compartments are filled with doped water which has conductivity  $\sigma = 0.037$  S/m and relative permittivity  $\epsilon_r = 80.4$ . Electrodes are attached to top and bottom of the inner two tubes. The phantom is placed with its longitudinal axis in the direction of  $\mathbf{B}_0$ .

As indicated in fig.3 (b),  $|\partial H_z / \partial z|$  is relatively small compared to  $|J_z|$ , especially in the center part where the current is highest. Therefore, the reconstructed current densities by the two different formulas are both very close to the simulated current distribution (fig. 3(c)).

The second model is a rectangular container filled with spatial varying conductive material (fig.4 (a)). The distribution of the electrical properties for one transverse plane is shown in fig.4 (b). As the electrodes are perpendicular to each other, current does not flow in one major direction all over the phantom. Therefore,  $|\partial H_z / \partial z| / |J_z|$  is significant in some regions as can be seen in fig.5 (b). Correspondingly,

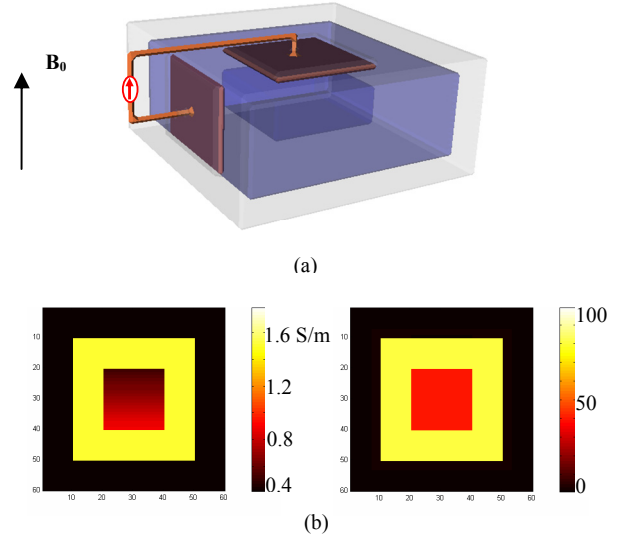


Fig. 4. (a) Simulation model 2  
(b) Conductivity (left) and relative permittivity (right) on a transverse plane (xy plane)

reconstructed current density along  $z$  direction by (9) is more accurate compared to the single orientation approximation in those regions (fig.5 (a) (c)).

## IV. EXPERIMENTAL TEST

### A. Methods

A multi-chamber phantom shown in fig.6 (a) was used in

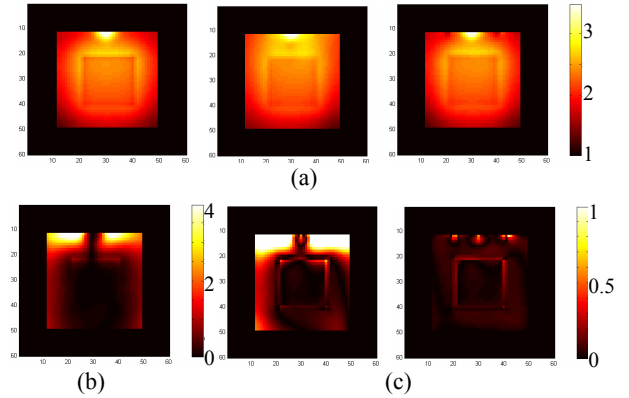


Fig. 5. Simulation results for model 2

- (a) Magnitude of  $J_z$  in logarithm scale
  - Left: directly from simulation
  - Middle: reconstructed by (5)
  - Right: reconstructed by (9)
- (b) map of  $|\partial H_z / \partial z| / |J_z|$
- (c) relative error of  $J_z$  magnitude for reconstruction by (5) (left) and (9) (right)

RF-CDI experiment. The structure is similar to simulation model 1. The center chamber was filled with solution with 0.9g/100ml NaCl and 0.1g/100ml CuSO<sub>4</sub>•5H<sub>2</sub>O giving  $\sigma \approx 1.48$  S/m and  $\epsilon_r \approx 80.4$ . The outer two chambers were filled with solution of same concentration of CuSO<sub>4</sub>•5H<sub>2</sub>O but no NaCl, which resulted in  $\sigma \approx 0.037$  S/m and  $\epsilon_r \approx 80.4$ . The phantom was placed in the imager with its longitudinal axis parallel to  $\mathbf{B}_0$  and then rotated to  $-\mathbf{B}_0$ . Data were collected for the two orientations by multi-slice RF-CDI sequence [6]. The imaging parameters were: field of view FOV = 0.24 m, frequency samples=256, phase encoding steps =256, slice thickness = 5.0 mm, slice gap = 2.5mm.

### B. Results

The reconstructed results are shown in fig.6 (b) and (c) for one slice. Current density magnitude and phase in fig.6 (b) and (c) were reconstructed by (5) and by (9) respectively. The overall patterns of the two sets of reconstructed current density are very similar to each other, because the current is expected to flow mainly in the axial direction of the phantom due to the electrode configuration.

However, the current density in fig.6 (c) is slightly more uniform within each chamber compared to (b). One reason for this is that one more set of data in (c) has an effect of signal averaging and hence the random noise influence is reduced.

## V. DISCUSSION

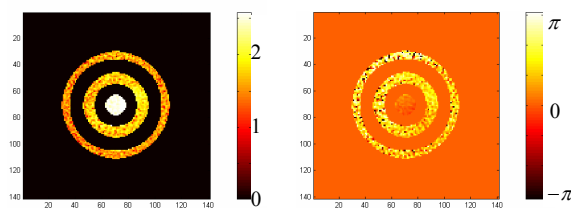
The approach to reconstruct current density vector through three orthogonal orientations could not be realized when RF-CDI was invented due to different coupling of the sample and the coil for different orientations in a small bore imager[4]. Although in the preliminary experiment shown in the last section, no obvious problem of coupling was noticed, the coupling effects should be further investigated. However, the issue of coupling might not be as serious as before. First, the bore of the imager is much bigger than the sample, which therefore occupies a small portion of the volume inside the body coil. Second, relative position between the sample and the coil after the 180-degree rotation is similar to the original relative position. Relative position between the sample and the coil experiences greater change for orthogonal rotations.

A more ambitious goal for RF-CDI is to extract the current density vector. By our approach in this paper, the transverse magnetic field components are estimated by (7) and (8). Since divergence of magnetic field is zero, one possible way is to compute  $H_z$  by spatial integration if  $H_z$  in a transverse plane is known. Once  $H_z$  is known, then  $J$  can be fully extracted.

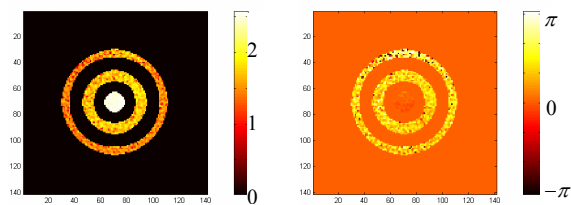
### ACKNOWLEDGMENT



(a)



(b)



(c)

Fig. 6. Phantom experiment

- (a) Photo of the phantom
- (b) Current density magnitude in logarithm scale (left) and phase (right) reconstructed by (5)
- (c) Current density magnitude in logarithm scale (left) and phase (right) reconstructed by (9)

Dinghui Wang would like to thank Dr. Greig C. Scott in Stanford University for his generous help in RF-CDI hardware, Ning Zhang for building RF current control box, Emidio Tarulli for designing the multi-chamber phantom and Dr. Costas D. Sarris in University of Toronto for providing the original Matlab code for 3-D FDTD simulation and NSERC for its support of the CDI project.

## REFERENCES

- [1] T.P. DeMonte, "Multi-slice current density imaging implementation and applications." M.S. Elec. Eng., Univ. Toronto, ON, Canada, 2000.
- [2] R. S. Yoon, A. Czaya, H. C. Kwan, and M. L. G. Joy, "Changes in the complex permittivity during spreading depression in rat cortex," *IEEE Trans. Biomed. Eng.*, vol. 46, no. 11, pp. 1330-1338, 1999.
- [3] G. C. Scott, K. Vigen, and A. Chen, "RF ablation current visualization at 0.5T," 13th ISMRM, pp. 151.
- [4] G. C. Scott, M. L. G. Joy, R. L. Armstrong, and R. M. Henkelman, "Electromagnetic considerations for RF current-density imaging," *IEEE Trans. Med. Imaging*, vol. 14, no. 3, pp. 515-524, 1995.
- [5] G. C. Scott, M. L. G. Joy, R. L. Armstrong, and R. M. Henkelman, "Rotating-frame RF current density imaging," *Magn. Reson. Med.*, vol. 33, no. 3, pp. 355-369, 1995.
- [6] D. Wang, T. P. DeMonte, and M. L. G. Joy, "Multi-slice radio frequency current density imaging," 13th ISMRM, pp. 2358.